Simulations of Materials: From Electrons to Friction

Uzi Landman; R. N. Barnett; W. D. Luedtke

Philosophical Transactions: Physical Sciences and Engineering, Vol. 341, No. 1661, New Methods for Modelling Processes within Solids and at their Surfaces (Nov. 16, 1992), 337-350.

Stable URL:
http://links.jstor.org/sici?sici=0962-8428%2819921116%29341%3A1661%3C337%3ASOMFET%3E2.0.CO%3B2-U

Philosophical Transactions: Physical Sciences and Engineering is currently published by The Royal Society.

Simulations of materials: from electrons to friction

By Uzi Landman, R. N. Barnett and W. D. Luedtke
School of Physics, Georgia Institute of Technology, Atlanta, Georgia 30332, U.S.A.

Quantum and classical molecular dynamics simulations are discussed, illustrating the applicability of computer-based modelling to a broad range of materials systems and phenomena. Case studies discussed include: quantum simulations of fission dynamics of charged atomic clusters and metallization of finite, small, alkali-halide crystals, classical molecular dynamics investigations of the consequences of interfacial adhesive interactions leading to the formation of intermetallic junctions, and the molecular mechanisms of capillary processes.

1. Introduction

Traditionally, modes of scientific investigations are classified, based on thematic, methodological or historical arguments, as theoretical or experimental in nature. The emergence of computers as high-powered research tools, and the development and proliferation of computer-based modelling and simulations, add a new dimension to our capabilities to explore natural phenomena and broaden our perspectives. Furthermore, by their nature computer-based modelling and simulations of materials are akin to theoretical experiments, where the physical system is represented by a theoretical model and a numerical algorithm, computational code, a computer, and various peripheral instruments (such as visualization devices) serve as the laboratory.

Computer simulations, where the evolution of a physical system is simulated, with refined temporal and spatial resolution, via a direct numerical solution of the equations of motion (quantum or classical) open new avenues in investigations of the microscopic origins of material phenomena (see articles in Catlow & Mackrodt 1982; Landau *et al.* 1988; Vitek & Srolovitz 1988; Nieminen *et al.* 1990). These methods alleviate certain of the major difficulties that hamper other theoretical approaches, particularly for complex systems such as those characterized by a large number of degrees of freedom, lack of symmetry, nonlinearities and complicated interactions. In addition to comparisons with experimental data, computer simulations can be used as a source of physical information, which is not accessible to laboratory experiments, and in some instances the computer experiment itself serves as a testing ground for theoretical concepts. Consequently, computer-based theoretical investigations of materials systems allow theorists to make contributions in explaining and elucidating the results of specific experiments, guide the developments of concepts, principles, and theories unifying a range of observations, and predict new behaviour.

Along with the opportunities and advantages presented by computer simulations, such studies do have certain limitations (mostly of a technical nature) and pitfalls associated with them. The main issues involved in critical assessment of simulation studies are: (i) the faithfulness of the simulation model, focusing mainly on our knowledge of the interaction potentials; (ii) the spatial dimension, i.e. finite size of the computational cell and imposed periodic boundary conditions in the case of

Phil. Trans. R. Soc. Lond. A (1992) **341**, 337–350
Printed in Great Britain

simulations of extended systems; and (iii) the finite time span of the simulation. The physical size and time extent used in a simulation are constrained by the available computational resources, and their adequacy depends upon characteristics of the specific system and phenomenon being studied, such as the state of aggregation, range of interactions, characteristic relaxation times, the scale of intrinsic spatial and temporal fluctuations and ambient conditions. The symbiotic relationship between large-scale computer-based modelling and computer technology benefits both areas. Indeed, in recent years the quest to simulate larger and more complex systems influenced the development of new computational strategies and computer architectures, and vice versa.

Basic understanding of the structure and dynamics of materials and their properties often requires knowledge on a microscopic level of the underlying energetics and interaction mechanisms, whose consequences we observe and measure. In this paper we discuss and demonstrate, using several case studies and various simulation techniques ranging from quantum to classical molecular dynamics applied to finite aggregates and extended systems, the wealth of information that can be obtained via quantum and classical simulations of materials, and the insights that such studies provide pertaining to fundamental as well as technology-related scientific issues.

2. Case studies

(a) *Quantum molecular dynamics: clusters*

Among the principal motivations for studies of clusters are a large number of observations that finite materials aggregates exhibit size-dependent physical and chemical properties, and the expectation that exploration of the systematics of such size effects and of their physical origins (both in the classical and quantum mechanical domains), would open avenues for understanding and elucidation of the size evolutionary patterns of materials properties, from the atomic and molecular scale to the condensed phase régime (see articles in Jena *et al.* 1987; Benedek *et al.* 1988).

(i) *Patterns and barriers for fission of charged small metal clusters*

Recent studies of metallic clusters (particularly of simple metals) unveiled systematic energetic, stability, spectral and fragmentation trends (see Barnett *et al.* 1991, and references therein), which bear close analogy to corresponding phenomena exhibited by atomic nuclei, suggesting an intriguing universality of the physical behaviour of finite size aggregates, though governed by interactions of differing spatial and energy scales.

To investigate energetic patterns and dynamics of fission of small Na_n^{+2} ($n \leqslant 12$) clusters, we have used our newly developed simulation method that combines classical molecular dynamics, or energy minimization, on the Born–Oppenheimer (BO) ground-state potential surface, with electronic structure calculations via the Kohn–Sham (KS) formulation of the local spin-density (LSD) functional method (Barnett *et al.* 1991; Rajagopal *et al* 1991). In dynamical simulations the ionic (classical) degrees of freedom evolve on the electronic BO surface, which is calculated after each classical step. Minimum energy structures were obtained by a steepest-descent method, starting from configurations selected from finite temperature simulations. Barrier heights and shapes were obtained by constrained energy minimization, with the centre-of-mass distance between the fragments specified.

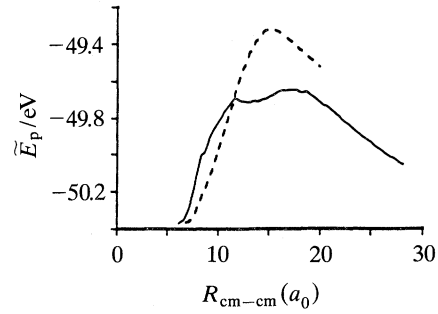

Figure 1. Potential energy against distance between the centre of mass for the fission $Na_{10}^{+2} \rightarrow Na_7^+ + Na_3^+$ (solid) and $Na_{10}^{+2} \rightarrow Na_9^+ + Na^+$ (dashed), obtained via constrained minimization of the LSD ground-state energy of the system.

Examination of the energetics of the clusters and of the various fragmentation channels reveals that in all cases the energetically favoured channel is $Na_n^{+2} \rightarrow Na_{n-3}^+ + Na_3^+$ ($n \leqslant 12$), i.e. asymmetric fission (except for $n = 6$), associated with shell closing in the product Na_3^+ cluster. Furthermore, our calculations show that for $n > 6$ fission involves energy barriers. The barriers for $n = 8$, 10 and 12 have been determined via constrained minimization to be: 0.16 eV, 0.71 eV and 0.29 eV for the energetically favoured channel, and larger barriers were found for the ejection of Na^+ from these clusters (0.43 eV and 1.03 eV for $n = 8$ and 10 respectively). The fission barriers for Na_{10}^{+2} are higher because of the closed-shell structure of this parent cluster.

The potential energies along the reaction coordinates for the energetically favoured channel and for Na^+ ejection, in the case of Na_{10}^{+2} are shown in figure 1. The most interesting feature seen from the figure is the rather unusual shape of the barrier for the favoured fission channel (also found for the asymmetric fragmentation of Na_{12}^{+2}). Although double-hump barriers have been long discussed in the theory of nuclear fission (Preston & Bhaduri 1975), to our knowledge this is the first time that they have been calculated in the context of asymmetric fission of charged atomic clusters (Barnett *et al.* 1991).

The existence of the double-humped barrier is reflected in the dynamics of the fission process of Na_{10}^{+2} displayed in figure 2, illustrating also the new capabilities afforded via quantum simulations for explorations of the dynamics of physical and chemical phenomena. This simulation started from a 600 K Na_{10} cluster from which two electrons were removed (requiring 11.23 eV) and 0.77 eV was added to the classical ionic kinetic energy. The variation of the centre-of-mass distance with time (figure 2*a*) exhibits a plateau for 750 fs $\leqslant t \leqslant$ 2000 fs (see also the behaviour of the electronic contribution to the potential energy of the system against time in figure 2*c*). The contours of the electronic charge density of the system (figure 2*d–f*), at selected times, and the corresponding cluster configurations (figure 2*g–i*), reveal that the fission process involves a precursor state that undergoes a structural isomerization before the eventual separation of the Na_7^+ and Na_3^+ fission products. In this context we remark that examination of the contributions of individual Kohn–Sham orbitals to the total density for the intermediate stage (figure 2*e*) reveals that the lowest-energy orbital (s-like) is localized on the Na_7^+ fragment, the second orbital is s-like localized on Na_3^+, the third is a p-like bonding orbital distributed over the two fragments, and the highest orbital is localized on the larger fragment.

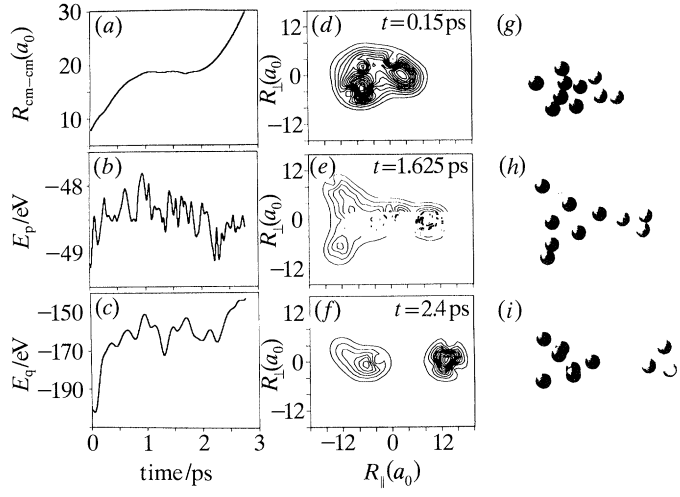

Figure 2. Fragmentation dynamics of Na_{10}^{+2}. (*a*)–(*c*) R_{cm-cm} between the fission products, total potential energy (E_p), and the electronic contribution (E_q) against time. (*d*)–(*f*) Contours of the total electronic charge distribution, calculated in the plane containing the two centres of masses. The R axis is parallel to R_{cm-cm}. (*g*)–(*i*) Ionic configurations for the times given in (*d*)–(*f*). Dark and light spheres represent ions in the large and small fragments respectively. Energy, distance, and time in units of eV, Bohr (a_0) and ps respectively.

(ii) *Metallization patterns of ionic clusters*

Investigations of localization modes, structure, dynamics and spectra of alkali-halide clusters containing multiple excess electrons (i.e. those electrons which substitute F^- anions in Na_nF_m, $m < n$) open new dimensions for studies of excess-electron localization and bonding in ionic clusters (Landman *et al.* 1985; Scharf *et al.* 1987; Rajagopal *et al.* 1990, 1991; for studies of modes and dynamics of electron and dielectron localization in water clusters see Barnett *et al.* 1990; Kaukonen *et al.* 1992), since the process of metallization of an initially stoichiometric ionic cluster (i.e. starting from an ionic cluster with $n = m$, and successively substituting anions by electrons, ultimately resulting in a neutral metallic cluster Na_n) may portray a transition from an insulating to a metallic state in a finite system. In this context we note that while transitions from F-centre to metallic behaviour have been observed in bulk molten alkali halides at high excess-metal concentrations, experimental data on metal-rich alkali-halide clusters are preliminary in nature (see references in Rajagopal *et al.* 1991).

In our BO–LSD simulations the inter-ionic interactions are described by the Born and Huang parametrized potentials which we have tested in previous studies, the interaction between the electrons and Na^+ is given by a norm-conserving pseudopotential, and a Coulomb repulsive potential describes the interaction between the electrons and F^- (Rajagopal *et al.* 1991).

We begin with a metallization sequence (MS) of a small cluster, Na_4F_m ($0 \leqslant m \leqslant 4$), which for $m = 4$ is a stable ionic cuboid and at the other extreme ($m = 0$) is a stable planar rhombohedral Na_4 cluster (see figure 3*a*–*e*). The structures exhibited by this MS demonstrate a systematic trend: structures of neutral small clusters belonging to a MS are of the same dimensionality and symmetry of the corresponding parent cluster, converting to the structure of the corresponding metal cluster upon complete metallization ($m = 0$). Furthermore, the excess electrons in these clusters,

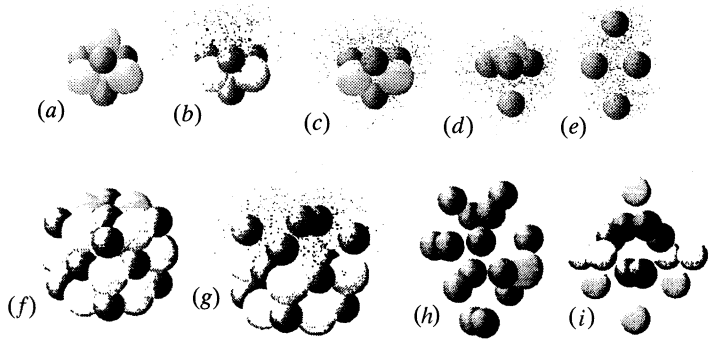

Figure 3. Optimal structures of Na_nF_m clusters. (*a*)–(*e*) MS for Na_4F_m ($0 \leqslant m \leqslant 4$). (*f*)–(*i*) Structures of $Na_{14}F_m$, for $m = 13$, 9, 1 and 0 respectively. Large and small spheres denote F^- and Na^+. Small dots represent the total excess electronic distribution.

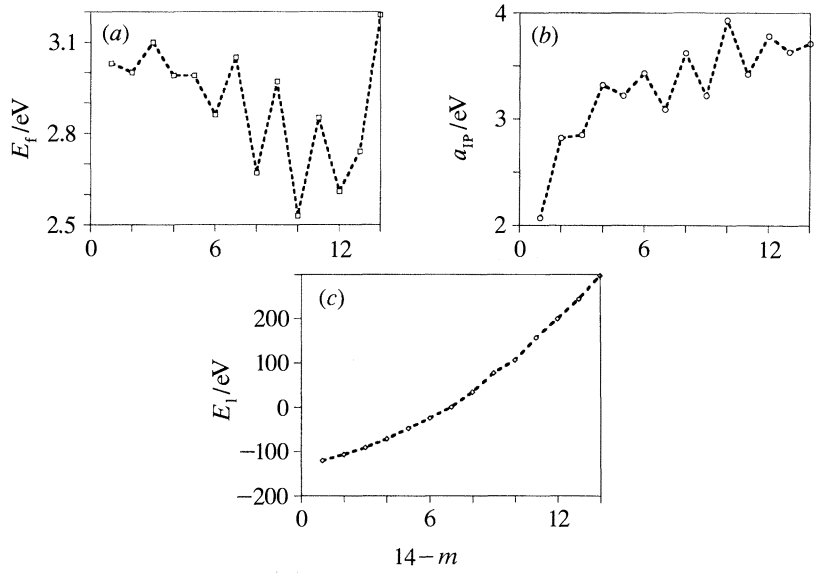

Figure 4. Energetics in the MS for $Na_{14}F_m$ against $14-m$, ($13 \geqslant m \geqslant 0$). Formation, adiabatic ionization, and ion-ion interaction energies in (*a*)–(*c*) respectively.

substituting for halide anions, maintain the cohesion and structural integrity of the clusters and their distributions exhibit a delocalized, metallic character (with the regions occupied by the remaining anions, i.e. for $0 < m < n$, excluded).

The MS for a larger cluster $Na_{14}F_m$ ($0 \leqslant m \leqslant 14$), whose $Na_{14}F_{13}$ member is a particularly stable cluster ($Na_{14}F_{13}^+$ is a 'magic number' ionic cluster, i.e. a $3 \times 3 \times 3$ filled cuboid structure, with three ions of alternating charges on an edge), exhibits another novel result: face (or atomic layer) metallization (segregation), as seen in figure 3*g*. The energetically optimal metallization sequence of this cluster proceeds via successive removal of neighbouring halogens from one face of the cluster, resulting (for $Na_{14}F_9$) in a segregated metal layer.

Examination of the pattern of metallization, and in particular the MS for $Na_{14}F_m$ (partly displayed in figure 3), reveals several trends. (i) The F-centre formation energies (E_f) (i.e. the difference between the total energies of Na_nF_{m-1} and Na_nF_m)

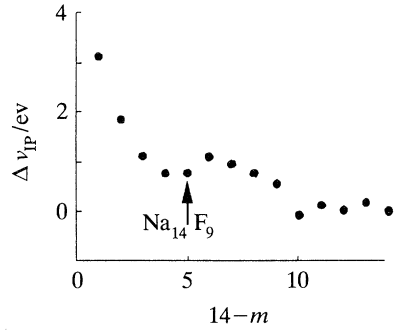

Figure 5. Δv_{IP} against $14-m$, $(13 \geqslant m \geqslant 0)$, for the MS of $Na_{14}F_m$. Note local minimum corresponding to $Na_{14}F_9$ and small values for $m \leqslant 4$, indicating enhanced metallic character.

are between 2.5 to 3.1 eV (figure 4). It is of interest that within a MS the formation energies, as well as the adiabatic (and vertical) ionization potentials, exhibit odd-even oscillations in $n-m$ indicating that perhaps these excess-metal systems may be regarded as composed of a 'metallic' component and a molecular-ionic one, symbolically represented as $Na_nF_m = Na_{n-m}(NaF)_m$. Our results (structural and energetic) for the bare metal and mixed clusters are in good agreement with experimental data and previous calculations, when available (Bonacic-Koutecky *et al.* 1991). (ii) A particularly interesting trend is exhibited by $\Delta v_{IP} = v_{IP}[Na_{n-m}] - v_{IP}[Na_{n-m}(NaF)_m]$, plotted in figure 5 against $n-m$ ($n = 14$ and $m = 1, 2, 3, \ldots$), which expresses the difference between the vertical ionization potential of a bare sodium cluster containing $n-m$ atoms and that of the mixed $Na_nF_m \equiv Na_{n-m}(NaF)_m$ cluster. Δv_{IP} may be regarded as a measure of metallic behaviour in the mixed cluster. As seen, for $n-m = 5$ (i.e. corresponding to $Na_{14}F_9$) Δv_{IP} attains a local minimum, suggesting enhanced metallic behaviour for the face-segregated cluster. Moreover, for $n-m \geqslant 10$ (i.e. $m \leqslant 4$), the perturbing effect of the ionic component of the cluster is small, and the electronic properties of the clusters approach those of the corresponding bare metal ones.

(*b*) *Adhesive junctions and capillary columns*

Understanding the atomistic mechanisms, energetics, structure and dynamics underlying the interactions and physical processes that occur when two materials are brought together (or separated) is fundamentally important to basic and applied problems such as adhesion, capillarity, contact formation, surface deformations, materials elastic and plastic response characteristics, materials hardness, micro- and nano-indentation, friction, lubrication, and wear, fracture and atomic-scale probing, modifications and manipulations of materials surfaces (see references in Landman *et al.* 1990, 1992; Landman & Luedtke 1991, 1992).

(i) *Adhesive intermetallic interfaces*

The first to introduce the notion of adhesive forces between material bodies in contact, and their contribution to the overall frictional resistance experienced by sliding bodies, was Desaguliers (1734, see also Dowson 1979), whose ideas on friction were conceived in the context of the role of surface finish, where he writes: '... the flat surfaces of metals or other Bodies may be so far polish'd as to increase Friction and this is a mechanical Paradox: but the reason will appear when we consider that the

Attraction of Cohesion becomes sensible as we bring the Surfaces of Bodies nearer and nearer to Contact'. These observations are incorporated in the current view that friction is the force required to shear intermetallic junctions plus the force required to plough the surface of the softer metal by the asperities on the harder surface (Bowden & Tabor 1973).

Application of newly developed theoretical and experimental (tip-based and surface-force apparatus) techniques (Israelachvili 1992; Sarid 1992; Murday & Colton 1990; Behm *et al.* 1989) promises to provide significant insights concerning the microscopic mechanisms and the role of surface forces in the formation of microcontacts and to enhance our understanding of fundamental issues pertaining to interfacial adherence, microindentation, surface deformations and the transition from elastic to elastoplastic or fully developed plastic response of materials, thin films, coatings, wetting and lubrication. Additionally, such studies in conjunction with atomistic investigations allow critical assessment of the range of validity of continuum-based theories of these phenomena and can inspire improved analytical formulations. Finally, knowledge of the interactions and atomic-scale processes occurring between small tips and materials surfaces, and their consequences, is of crucial importance to optimize, control, interpret and design experiments using novel tip-based microscopies.

As an illustration of recent progress in this area we show in figure 6*a* (solid line) the force between a nickel tip and Au(001) surface as they approach each other and are subsequently separated (Landman *et al.* 1990). In these large-scale molecular dynamical (MD) simulations the EAM potentials (Adams *et al.* 1989) are used for a system consisting of eight dynamic and three static Au(001) layers, with 450 atoms per layer, and the Ni tip consists of a bottom layer of 72 atoms exposing a (001) facet, the next layer consists of 128 atoms and the remaining six layers contain 200 dynamic atoms each. This gives the tip an effective radius of curvature of about 30 Å†. The static holder of the tip (rigid cantilever) consists of 1176 atoms arranged in three (001) layers. All simulations were performed at 300 K, and following equilibration motion of the tip in the normal direction relative to the substrate occurs via changing the position of the tip-holder assembly in increments of 0.25 Å, and after each increment fully relaxing the system, i.e. dynamically evolving until no discernable variations in system properties are observed beyond natural fluctuations.

The main features observed from figure 6*a* (and in accompanying atomic-force microscopy experiments (Landman *et al.* 1990)) are the following.

1. The onset of an instability, signified by a sharp increase in the attraction between the tip and the substrate, occurring at a distance $d_{ts} \approx 4.20$ Å, between the bottom-most atomic layer of the tip and the top-most atomic layer of the gold surface. This instability, which results in a jump-to-contact (JC) phenomenon, occurs via a plastic deformation of the Au(001) surface in the region under the tip, involving displacement of atoms in that region by about 2 Å in 1 ps (after the JC occurs the spacing between the bottom layer of the Ni tip and the adherent (wetting) layer of Au atoms decreases to 2.1 Å from a value of 4.2 Å before JC).

The jump-to-contact phenomenon in metallic systems is driven by the marked tendency of the atoms at the interfacial regions of the tip and substrate materials to optimize their embedding energies (which are density dependent, deriving from the tails of the atomic electronic charge densities) while maintaining their individual

† 1 Å = 10^{-10} m = 10^{-1} nm.

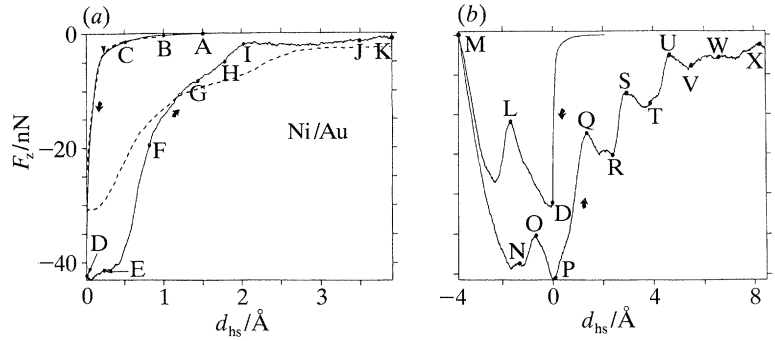

Figure 6. Calculated force on the tip atoms, F_z, against tip-to-sample distance d_{hs}, between a Ni tip and an Au sample for: (*a*) approach and jump-to-contact followed by separation; (*b*) approach, jump-to-contact, indentation, and subsequent separation; d_{hs} denotes the distance between the rigid tip-holder assembly and the static substrate of the Au surface ($d_{hs} = 0$ at the jump-to-contact point marked D). The capital letters on the curves denote the actual distances, d_{ts}, between the bottom part of the Ni tip and the Au surface; in (*a*) A = 5.7 Å, B = 5.2 Å, C = 4.7 Å, D = 3.8 Å, E = 4.4 Å, F = 4.85 Å, G = 5.5 Å, H = 5.9 Å, I = 6.2 Å, J = 7.5 Å and K = 8.0 Å; in (*b*) D = 3.8 Å, L = 2.4, M = 0.8 Å, N = 2.6 Å, O = 3.0 Å, P = 3.8 Å, Q = 5.4 Å, R = 6.4 Å, S = 7.0 Å, T = 7.7 Å, U = 9.1 Å, V = 9.6 Å, W = 10.5 Å, and X = 12.8 Å. Forces in units of nanonewtons, and distance in ångströms.

material cohesive binding (in the Ni and Au) albeit strained due to the deformation caused by the atomic displacements during the JC process. In this context we note the difference between the surface energies of the two metals, with the one for Ni markedly larger than that of Au, and the differences in their mechanical properties (for example, the elastic moduli are 21×10^{10} and 8.2×10^{10} N m^{-2} for Ni and Au respectively).

Additional insight into the JC process is provided by the local hydrostatic pressure and stress distribution in the materials (evaluated from the atomic stress tensors) after contact formation. Both the structural deformation profile of the system and the stress distribution which we find in our atomistic MD simulations are similar, in general terms, to those described by certain modern contact mechanics theories (see review in Israelachvili 1992; Burnham *et al.* 1991; articles in Pollock & Singer 1992; see also references in Landman *et al.* 1990), where the influence of adhesive interactions is included, indicating the applicability of such continuum descriptions even to systems characterized by rather small spatial dimensions.

2. Reversal of the direction of the tip motion relative to the substrate starting from the point of adhesive contact (point D in figure 6*a*) results in a marked hysteresis (we note that separating the two before contact results in no hysteresis). The hysteresis is a consequence of the adhesive bonding between the two materials, which upon retraction of the tip results in the formation of a connective neck, with a monolayer of gold atoms coating (wetting) the retracted Ni tip.

It is of interest to note that repeating the process but using the gold coated nickel tip, results again in a JC instability (though of reduced magnitude) and hysteresis upon retraction (see figure 6*a*, dashed line). However, while plastic deformation of the surface and neck formation were observed during the lift-off process, no gold atom transfer to the coated tip was observed (Landman *et al.* 1992).

Allowing the tip to advance past the jump-to-contact point, that is indenting the surface, results in the force against distance curve recorded in figure 6*b*. Of particular

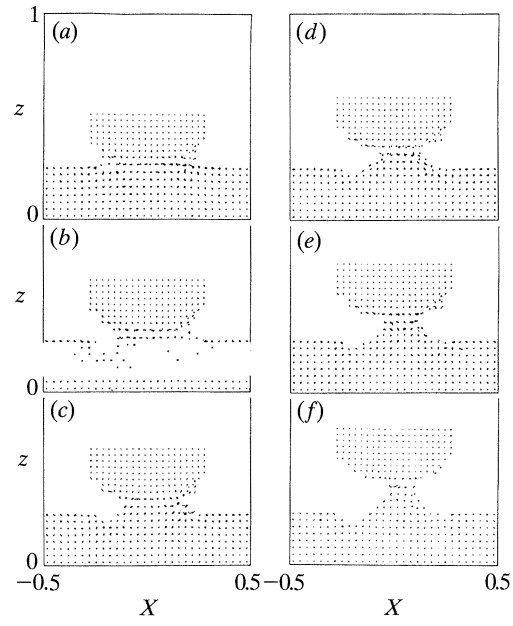

Figure 7. Atomic configurations in slices through the system illustrating the formation of a connective neck between the Ni tip and the Au substrate during separation following indentation. The Ni tip occupies the topmost eight layers. The configurations (*a*)–(*f*) correspond to the stages marked O, Q, S, U, W, and X in figure 6*b*. Note the crystalline structure of the neck. Successive elongations of the neck, upon increased separation between the tip-holder assembly and the substrate, occur via structural transformation resulting in successive addition of layers in the neck accompanied by narrowing (i.e. reduction in cross-sectional area of the neck). Distance in units of X and Z, with $X = 1$ and $Z = 1$ corresponding to 61.2 Å.

interest are the oscillations in the force upon retraction from the point of zero force (point M in figure 6*b*), associated with the formation and elongation of a connective junction consisting mainly of gold atoms (see figure 7). Further insight into the microscopic mechanism of elongation of the connective neck can be gained via consideration of the variation of the second invariant of the stress deviator, J_2, which is proportional to the stored strain energy and is related to the von Mises shear strain-energy criterion for the onset of plastic yielding (Dieter 1967). Such analysis reveals that between each of the elongation events (i.e. layer additions, points marked Q, S, U, W and X) the initial response of the system to the strain induced by the increased separation is mainly elastic (segments OP, QR, ST, UV in figure 6*b*) accompanied by a gradual increase of the stored strain energy. The onsets of the stages of structural rearrangements are found to be correlated with a critical maximum value of $\sqrt{J_2}$ of about 3 GPa (occurring for states at the end of the intervals marked OP, QR, ST and UV in figure 6*b*), localized in the neck in the region of the ensuing structural transformation. After each of the elongation events the maximum value of $\sqrt{J_2}$ (for the states marked Q, S, U, W and X in figure 6*b*) drops to approximately 2 GPa.

The theoretically predicted increased hysteresis upon tip–substrate separation following indentation, relative to that found after contact (compare figure 6*a*, *b*), is also observed experimentally (Landman *et al.* 1990). While in the original experiments the non-monotonic features found in the simulations (figure 6*b*) were

not discernible in the force against distance data, they have been observed in recent experiments performed under ultra-high vacuum conditions (C. M. Mate, personal communication).

(ii) *Capillary junctions*

Our discussion up to this point was confined to the interaction between material tips and bare crystalline substrates. Motivated by the fundamental and practical importance of understanding the properties of adsorbed molecularly thin films and phenomena occurring when films are confined between two solid surfaces, pertaining to diverse fields such as fluid-film lubrication, prevention of degradation and wear, wetting, spreading and drainage, the mechanical response and relaxation of adsorbed organic films, and AFM measurements, we have initiated most recently investigations of such systems (Landman *et al.* 1992; Landman & Luedtke 1992). Among the issues that we attempt to address are the structure, dynamics, and response of confined complex films, their rheological properties, and modification which they may cause to adhesive and tribological phenomena, such as inhibition of jump-to-contact instabilities and prevention of contact junction formation.

The molecular films that we studied, *n*-hexadecane ($C_{16}H_{34}$), were modelled by interaction potentials developed by Ryckaert & Bellemans (1978), which have been used before in investigations of the thermodynamic, structural and rheological properties of bulk liquid *n*-alkanes, and adsorbed hexadecane films of variable thickness (butane and decane (Leggeter & Tildesley 1989; Xia *et al.* 1992; Ribarsky & Landman 1992)). The metallic substrate (Au) and tip (Ni) were modeled using the EAM potentials and the interactions between the *n*-hexadecane molecules and the metallic tip and substrate were described using LJ potentials, determined by fitting to experimentally estimated adsorption energies (Xia *et al.* 1992; Landman & Luedtke 1992).

Studies of the response of the system revealed (Landman *et al.* 1992) that lowering of a faceted nickel tip towards a gold surface covered by a thin adsorbed *n*-hexadecane film results first in small attraction between the film and the tip followed, upon further lowering of the tip, by ordering (layering) of the molecular film (see below). During continued approach of the tip toward the surface the total interaction between the tip and the substrate (metal plus film) is repulsive, and the process is accompanied by molecular drainage from the region directly under the tip, wetting of the sides of the tip, and ordering of the adsorbed molecular monolayer under the tip. Further lowering of the tip is accompanied by inward deformation of the substrate and eventual formation of intermetallic contact (occurring via displacement of surface gold atoms towards the tip) which is accompanied by partial molecular drainage and results in a net attractive force on the tip. We note that, unlike the case of the bare metal interface discussed before, formation of contact in the presence of an adsorbed film required the application of a relatively high load.

The last case study we discuss illustrates the consequences of tip–sample interactions in investigations of capillary phenomena occurring upon approach and subsequent retraction of a blunted tip, to and from a liquid alkane film (Landman & Luedtke 1992). In this study the simulated system is composed of a large gold static substrate, a static nickel tip, and a film of alkane molecules whose number is controlled such as to approximately conserve the chemical potential of the system (i.e. a pseudo grand-canonical molecular dynamics simulation where the thickness of the adsorbed molecular liquid film in regions away from the tip is monitored

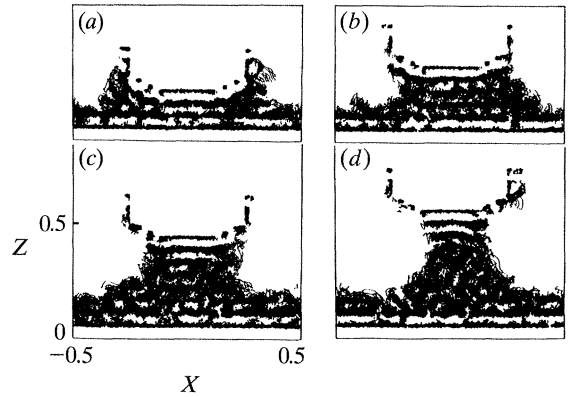

Figure 8. Short-time trajectories, obtained via MD simulations at 350 K, of hexadecane molecules forming a capillary column between a gold substrate and a nickel tip at four stages of the tip-lifting process (trajectories were plotted in a 23 Å wide slice through the middle of the system). The distances between the tip and the substrate for the configurations shown in (*a*)–(*d*) are d_{ts} = 19.3 Å, 28.1 Å, 36.9 Å and 45.7 Å, correspondingly. The length scale of the calculational cell, which was periodically repeated along the x and y directions is 77.5 Å.

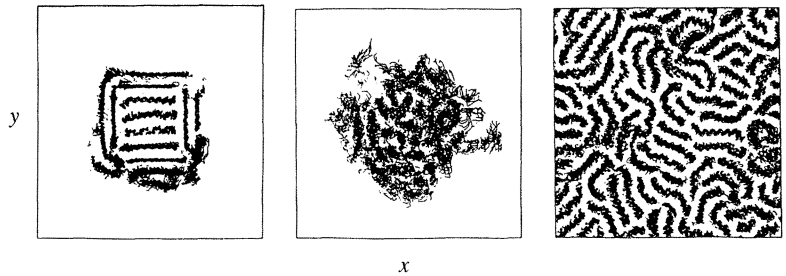

Figure 9. Short-time trajectories of hexadecane molecules in three regions of the capillary column formed between a gold surface and a nickel tip separated by 36.9 Å (corresponding to the configuration shown in figure 8*c*). The bottom configuration corresponding to the region of the film closest to the gold surface illustrates preferential orientation of the molecules parallel to the surface and islands of intermolecular ordering. The middle panel illustrates lack of order in the middle of the liquid junction, while the molecular configuration shown at top, corresponding to a region closest to the bottom of the nickel tip, illustrates a high degree of preferential parallel molecular orientation and intermolecular order. Length scale as in figure 8.

throughout the wetting and growth of the capillary liquid column, and molecules are added at the edges of the edges of the computational cell to compensate for those that were pulled up toward the tip by the adhesive and capillary forces).

Four configurations of the alkane film are shown in figure 8, each corresponding to an equilibrium state of the system at a given separation between the tip and the surface. The configurations shown in figure 8*a*, *b* correspond to distances d_{ts} = 19.3 Å and d_{ts} = 28.1 Å between the bottom layer of the Ni tip and the topmost layer of the gold surface. As seen in these stages the liquid film in the region under the tip consists of four and six distinct layers, respectively, while the arrangement of molecules on the sides of the liquid-junction is less ordered, receding to a two-layer adsorbed film further away from the tip. At this point it is of interest to note that the degree of layering is found to exhibit a marked sensitivity to the distance d_{ts} between the tip and the substrate, maximizing when d_{ts} is commensurate with an integral number of

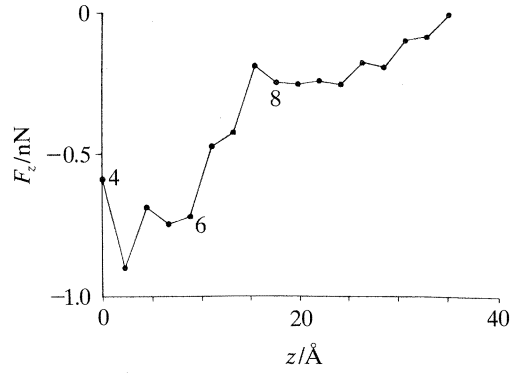

Figure 10. Normal force on the nickel tip (in nN) against the distance between the tip and the gold surface, Z (in Å) with the origin taken as that corresponding to a four-layer capillary column (see figure 8*a*). Dots indicate distances for which the system was relaxed during the tip-lifting process. The numbers on the graph denote the number of layers in the capillary column (for the eight-layer column this number is ambiguous due to disordering in the middle part, see figure 8*c*).

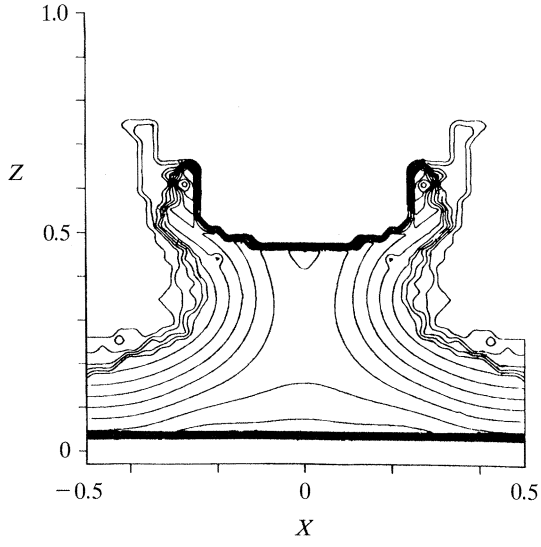

Figure 11. Segmental density contours for the 36.9 Å high capillary column (see figure 8*c*) of hexadecane molecules, obtained via MD simulations at 350 K. The density at the middle (core) of the column is 0.033 segments Å^{-3}, which is the same as that of bulk hexadecane at the above temperature. The spacing between contour lines $\Delta\rho = 0.003$ segments Å^{-3}. The linear dimension along the x and z directions is 77.5 Å.

liquid layer spacings. Upon raising the tip to a distance $d_{ts} = 36.9$ Å (figure 8*c*) and subsequently to $d_{ts} = 45.7$ Å (figure 8*d*) the layered nature of the confined film (in the middle region of the capillary column) diminishes. The short-time trajectories of hexadecane molecules at the tip, middle and bottom of the liquid column of height 36.9 Å, shown in figure 9, illustrate the ordered nature of the film next to the tip and surface, and reduced order at the middle of the capillary junction.

The transition from a layered to a partially layered liquid junction is reflected in the force against distance curve shown in figure 10, portraying the energetics of the system (compare with figure 6, corresponding to the elongation of solid junctions,

where no such transition was observed). Clearly, the force required in order to elongate the column in the height range corresponding to layered configurations is significantly larger than that needed to separate the two interfaces when part of the liquid junction between them acquires liquid-like properties.

Finally, such simulations allow a quantitative analysis of the density distribution and energetics of the capillary structures on the molecular level, as illustrated in figure 11, where contours of the segmental density for a capillary column of height $d_{ts} = 36.9$ Å, are shown. First, it is of interest to note that even for such microscopic capillary junctions the density at the core achieves that of the bulk liquid at the same temperature (T = 350 K). Secondly, the density profile of the column exhibits a gradual decrease from the core outwards. The radii of curvature determined from such plots together with contours of the molecular pressure tensor distribution in the column, allow a direct microscopic evaluation of the Young–Laplace equation (Luedtke & Landman 1992) and disjoining pressure of the film, and provide detailed molecular-level guidance for the analysis of AFM data (Mate *et al.* 1989; Mate & Novotny 1991).

Research supported by U.S. Department of Energy, the Air Force Office of Scientific Research and the NSF. Calculations performed at the Florida State Computer Center and at NERSC, Livermore, California, through a grant by DOE.

References

Adams, J. B., Foiles, S. M. & Wolfer, W. G. 1989 Self-diffusion and impurity diffusion of fcc metals using the five-frequency model and the embedded atom method. *J. Mater. Res.* **4**, 102–112.

Barnett, R. N., Landman, U., Makov, G. & Nitzan, A. 1990 Theoretical studies of the spectroscopy of excess electrons in water clusters. *J. chem. Phys.* **93**, 6226–6238.

Barnett, R. N., Landman, U. & Rajagopal, G. 1991 Patterns and barriers for fission of charged small metal clusters. *Phys. Rev. Lett.* **67**, 3058–3061.

Behm, R. J., Garcia, N. & Rohrer, H. (eds) 1989 *Scanning tunneling microscopy and related methods.* Dordrecht: Kluwer.

Benedek, G., Martin, T. P. & Pacchioni, G. (eds) 1988 *Elemental and molecular clusters.* Berlin: Springer.

Bonacic-Koutecky, V., Fantucci, P. & Koutecky, J. 1991 Quantum chemistry of small clusters of elements of groups Ia, Ib and IIa: fundamental concepts, predictions and interpretation of experiment. *Chem. Rev.* **91**, 1035–1070.

Bowden, F. P. & Tabor, D. 1973 *Friction.* Garden City, New York: Anchor Press / Doubleday.

Burnham, N. A., Colton, R. J. & Pollock, H. M. 1991 Interpretation issues in force microscopy. *J. Vac. Sci. Technol.* A **9**, 2548–2556.

Catlow, C. R. A. & Mackrodt, W. C. (eds) 1982 *Computer simulations of solids.* Berlin: Springer.

Desaguliers, J. T. 1734 *A course of experimental philosophy*, vols 1 and 2. London.

Dieter, G. 1967 *Mechanical metallurgy.* New York: McGraw-Hill.

Dowson, D. 1979 *History of tribology.* London: Longman.

Israelachvili, J. N. 1992 *Intermolecular and surface forces* (2nd edn). London: Academic Press.

Jena, P., Rao, B. K. & Khanna, S. N. (eds) 1987 *Physics and chemistry of small clusters.* New York: Plenum.

Kaukonen, H.-P., Barnett, R. N. & Landman, U. 1992 Dielectrons in water clusters. *J. chem. Phys.* **97**, 1365–1377.

Landman, U. & Luedtke, W. D. 1991 Nanomechanics and dynamics of tip–substrate interactions. *J. Vac. Sci. Technol.* B **9**, 414–423.

Landman, U. & Luedtke, W. D. 1992 Consequences of tip–substrate interactions. In *Scanning microscopy III* (ed. H.-J. Guntherodt & R. Wiesendanger). Berlin: Springer.

Landau, D. P., Mon, K. K. & Schuttler, H.-B. (eds) 1988 *Computer simulation studies in condensed matter physics.* Berlin: Springer.

Landman, U., Scharf, D. & Jortner, J. 1985 Electron localization in alkali-halide clusters. *Phys. Rev. Lett.* **54**, 1860–1863.

Landman, U., Luedtke, W. D., Burnham, N. A. & Colton, J. 1990 Atomistic mechanisms and dynamics of adhesion, nanoindentation, and fracture. *Science, Wash.* **248**, 454–461.

Landman, U., Luedtke, W. D. & Ringer, E. M. 1992 Atomistic mechanisms of adhesive contact formation and interfacial processes. *Wear* **153**, 3–30.

Leggetter, S. & Tildesley, D. J. 1989 The computer simulations of adsorbed hydrocarbons. *Molec. Phys.* **68**, 519–546.

Luedtke, W. D. & Landman, U. 1992 Solid and liquid junctions. *Comp. Mater. Sci.* **1** (In the press.)

Mate, C. M., Lorenz, M. R. & Novotny, V. J. 1989 Atomic force microscopy of polymeric liquid films. *J. chem. Phys.* **90**, 7550–7555.

Mate, C. M. & Novotny, V. J. 1991 Molecular conformation and disjoining pressure of polymeric liquid films. *J. chem. Phys.* **94**, 8420–8427.

Murday, J. S. & Colton, R. J. 1990 Proximal probes: techniques for measuring at the nanometer scale. *Mater. Sci. Engng* B **6**, 77–85.

Nieminen, R. M., Puska, M. J. & Manninen, M. J. (eds) 1990 *Many-atom interactions in solids.* Berlin: Springer.

Pollock, H. M. & Singer, I. (eds) 1992 *Fundamentals of tribology.* Dordrecht: Kluwer.

Preston, M. A. & Bhaduri, R. K. 1975 *Structure of the nucleus*, p. 589. Reading, Massachusetts: Addison-Wesley.

Rajagopal, G., Barnett, R. N., Nitzan, A., Landman, U., Honea, E. C., Labastie, P., Homer, M. L. & Whettne, R. L. 1990 Optical spectra of localized excess electrons in alkali halide clusters. *Phys. Rev. Lett.* **64**, 2933–2936.

Rajagopal, G., Barnett, R. N. & Landman, U. 1991 Metallization of ionic clusters. *Phys. Rev. Lett.* **67**, 727–730.

Ribarsky, M. W. & Landman, U. 1992 Structure and dynamics of n-alkanes confined by solid surfaces I. Stationary crystalline boundaries. *J. chem. Phys.* **97**, 1937–1949.

Ryckaert, J. P. & Bellemans, A. 1978 Molecular dynamics of liquid alkanes. *Faraday Discuss. chem. Soc.* **66**, 95–106.

Sarid, D. 1991 *Scanning force microscopy.* New York: Oxford University Press.

Scharf, D., Jortner, J. & Landman, U. 1987 Cluster isomerization induced by electron attachment. *J. chem. Phys.* **87**, 2716–2723.

Vitek, V. & Srolovitz, D. J. (eds) 1988 *Atomic simulation of materials: beyond pair potentials.* New York: Plenum.

Xia, T. K., Ouyang, J., Ribarsky, M. W. & Landman, U. 1992 Interfacial alkane films. *Phys. Rev. Lett.* (In the press.)